HHS Public Access

Author manuscript

Magn Reson Med. Author manuscript; available in PMC 2014 October 08.

Published in final edited form as:

Magn Reson Med. 2014 March ; 71(3): 978–989. doi:10.1002/mrm.24750.

Vessel-specific quantification of blood oxygenation with T2-Relaxation-Under-Phase-Contrast (TRU-PC) MRI

Lisa C. Krishnamurthy[1,2], **Peiying Liu**[1], **Yulin Ge**[3], and **Hanzhang Lu**[1]

[1]Advanced Imaging Research Center, University of Texas Southwestern Medical Center, Dallas, TX, USA

[2]Department. of Biomedical Engineering, University of Texas at Arlington, Arlington, TX, USA

[3]Department of Radiology, New York University Langone Medical Center, New York, NY, USA

Abstract

Purpose—Measurement of venous oxygenation (Y_v) is a critical step toward quantitative assessment of brain oxygen metabolism, a key index in many brain disorders. The present study aims to develop a non-invasive, rapid, and reproducible method to measure Y_v in a vessel-specific manner.

Theory—The method, T2-Relaxation-Under-Phase-Contrast (TRU-PC) MRI, utilizes complex subtraction of phase-contrast to isolate pure blood signal, applies non-slice-selective T2-preparation to measure T_2, and converts T_2 to oxygenation using a calibration plot.

Methods—Following feasibility demonstration, several technical aspects were examined, including validation with an established global Y_v technique, test-retest reproducibility, sensitivity to detect oxygenation changes due to hypoxia and caffeine challenges, applicability of EPI acquisition to shorten scan duration, and ability to study veins with a caliber of 1–2 mm.

Results—TRU-PC was able to simultaneously measure Y_v in all major veins in the brain, including sagittal sinus, straight sinus, great vein, and internal cerebral vein. TRU-PC results showed an excellent agreement with the reference technique, high sensitivity to oxygenation changes, and test-retest variability of 3.5±1.0%. The use of segmented-EPI was able to reduce the scan duration to 1.5 minutes. It was also feasible to study pial veins and deep veins.

Conclusion—TRU-PC MRI is a promising technique for vessel-specific oxygenation measurement.

Keywords

blood oxygen saturation; small vessel; TRU-PC; TRUST; $CMRO_2$

Corresponding author: Hanzhang Lu, Ph.D., Advanced Imaging Research Center, Psychiatry, Radiology, UT Southwestern Medical Center, 5323 Harry Hines Boulevard, Dallas, Texas 75390, Office Phone: 214-645-2761, Office Fax: 214-645-2885, hanzhang.lu@utsouthwestern.edu.

Introduction

Measurement of human brain metabolism is of great importance in brain disorders and in functional brain imaging, but for decades it has been a niche market of Positron Emission Tomography (PET) (1–3). Recent advances in MR technologies have allowed the quantification of cerebral metabolic rate of oxygen ($CMRO_2$) on a whole-brain level (4–7). However, regional measurement of $CMRO_2$ is still difficult (8). This is because methods that are able to evaluate venous blood oxygenation (Y_v) on a regional basis are largely absent. To this end, several potential approaches have been proposed: quantitative Blood Oxygenation Level Dependent (qBOLD) contrast (9–13), susceptibility phase based techniques (4,5,14,15), quantitative susceptibility mapping (QSM) methods (16,17), and intravascular blood T_2 measurements (6,18–20). Traditionally, the qBOLD method was the only regional $CMRO_2$ measure, though the drawback was the complicated modeling and the high SNR required to fit for Y_v. Phase based techniques such as the Phase-based Regional Oxygen Metabolism (PROM) method (15) can image certain small vessels, but requires the assumption of vessel orientation, and is relatively sensitive to field inhomogeneity. The QSM method is a promising approach based on deconvolution of the field map, although theoretical considerations are still being made to improve the solution to the inverse problem (16,17).

Intravascular T_2-based methods rely on a simple and calibratable relationship between blood T_2 and oxygenation, thus representing a relatively straightforward approach to quantify Y_v. Insofar, the greatest challenge that this method is faced with is to isolate pure blood signal from the surrounding tissue. This problem was partly addressed by the development of T2-Relaxation-Under-Spin-Tagging (TRUST) MRI (6), which applies a spin-tagging principle like Arterial-Spin-Labeling (ASL) (21), but on the venous side. By subtraction of control and label images, pure venous blood signal is isolated. Due to its simplicity and robustness, TRUST has been increasingly used in several neurodegenerative diseases that involve the whole brain including Alzheimer's disease and multiple sclerosis (22) for evaluation of oxygen metabolism. However, its most resounding critique is the lack of spatial information since it solely measures Y_v at a single point of the brain, providing only a global value.

Two other spin-tagging based Y_v methods, QUantitative Imaging of eXtraction of oxygen and TIssue Consumption (QUIXOTIC) (23) and Velocity-Selective Excitation and Arterial Nulling (VSEAN) (24), have since been proposed to provide the separation of blood from tissue signal in the microvasculature. Though these techniques are elegant in many aspects, QUIXOTIC is plagued by residual errors from eddy currents, and VSEAN may contain contributions from arterial and capillary blood (24). Thus, regional measure of Y_v using the spin-tagging techniques remains challenging.

We therefore sought to identify a new approach to separate blood signal from static tissue. This approach employs a phase-contrast principle to isolate pure blood signal in specific veins, measures the T_2 value of the blood signal using T_2-prepration modules, and converts the estimated T_2 to oxygenation via a calibration plot. We dubbed this technique T_2-Relaxation-Under-Phase-Contrast (TRU-PC) MRI.

We conducted a series of experimental studies on the TRU-PC sequence. We first demonstrated the feasibility of the proposed method in estimating regional Y_v values and investigated the reproducibility of the measure. The TRU-PC results were also compared to a validated whole-brain method, TRUST MRI (6). Furthermore, TRU-PC's sensitivity in detecting changes in blood oxygenation was studied using hypoxic gas breathing challenge and caffeine ingestion. Sequence parameter optimization was conducted to reduce scan duration while maintaining measurement reliability. Finally, the capability of this technique to measure blood oxygen content in small vessels (1–2 mm in diameter) was demonstrated. A preliminary form of this report has been presented in abstract format (25).

Theory

The TRU-PC pulse sequence and the relevant magnetization vectors are shown in Figure 1. As seen in Figure 1a, the key principle of TRU-PC is the combination of a T_2-preparation (red box) with phase-contrast MRI (green box). The phase-contrast module serves to isolate pure venous blood signal, and the T_2-preparation modulates T_2-weighting of the signal. A post-saturation pulse is applied following the signal acquisition to remove spin history (blue box), so that the magnetization can be accurately modeled regardless of the previous RF pulses experienced.

The principle of phase-contrast in isolating blood signal is well established (26–29). Briefly, let us consider a voxel containing both static tissue and flowing blood. The total magnetization of the voxel will be the vector summation of both compartments. The TRU-PC sequence uses a bipolar gradient (green box) to modulate the phase of the magnetization such that spins moving at a velocity (blue vectors in Figure 1b) will accumulate a phase, $\Phi=\gamma m_1 v$, whereas static spins (yellow vectors in Figure 1b) will not accumulate any phase (27). Here γ is the gyromagnetic ratio, m_1 is the first moment of the gradient waveform, and v is the velocity. In the next scan (denoted as "−" in Figure 1), by flipping the polarity of the gradients (shown as gray trapezoids in Figure 1a), the phase of the moving spins will be $-\Phi$. The complex difference, CD (bottom row, Figure 1b), of these two signals will then cancel out the static tissue signal (26,29). Thus, only the moving blood signal is measured, the signal intensity of which is $2M_{blood}|\sin(\Phi)|$. In practice, one often defines a maximum encoding velocity, V_{enc}, such that $\gamma m_1 V_{enc}=\pi/2$. The complex difference signal can then be written as (27):

$$CD=2M_{blood}\left|\sin\left(\frac{\pi v}{2V_{enc}}\right)\right| \quad [1]$$

The term, M_{blood}, follows magnetization evolution as determined by the other components in the pulse sequence and the simulation results are shown in Figure 1c. At the time when the excitation RF pulse is applied, M_{blood} is given by:

$$M_{blood}(eTE)=M_0\cdot f_{blood}\cdot\left(1-e^{-\frac{RT}{T_{1,blood}}}\right)\cdot e^{-\frac{eTE}{T_{2,blood}}} \quad [2]$$

where M_0 is the equilibrium magnetization, f_{blood} is the partial volume fraction of blood in the voxel, Recovery Time (RT) is the time gap between post-saturation RF pulse and the beginning of the next TR (Figure 1a), and effective TE (eTE) is the duration of the T_2-preparation (Figure 1a). Replacing the term M_{blood} in Eq. [1] with Eq. [2], the TRU-PC complex difference signal can be written as:

$$CD=2M_0 \cdot f_{blood} \cdot \left|\sin\left(\frac{\pi v}{2V_{enc}}\right)\right| \cdot \left(1-e^{-\frac{RT}{T_{1,blood}}}\right) \cdot e^{-\frac{eTE}{T_{2,blood}}}. \quad [3]$$

One can therefore acquire the signals at a range of eTE values to obtain a fitting for $T_{2,blood}$. To ensure that the other terms in Eq. [3] do not change with eTE, the repetition time (TR) is adjusted for every eTE so that the RT is constant throughout the experiment (Note: $RT=TR-eTE-T_{acq}$).

In order for Eq. [3] to be valid for both static spins and fresh spins flowing into the imaging volume, a non-slice-selective saturation RF pulse is applied after each acquisition. This pulse is termed post-saturation (blue box, Figure 1a), and is applied to reset the magnetization of all spins to be zero. Use of a post-saturation pulse has been employed in other techniques to reset either the arterial or whole brain-signal (30–33).

Methods

General

Experiments were performed on a total of 36 healthy subjects (age 33 ± 10 years, range 20–59, 20 Males, 16 Females) using a 3 Tesla MRI scanner (Philips Medical Systems, Best, The Netherlands). The protocol was approved by the University of Texas Southwestern Medical Center's Institutional Review Board. The body coil was used for RF transmission, and a 32-channel head coil was used for receiving. The subjects were instructed not to fall asleep (verified after the scan) and to remain motionless. Foam padding was placed around the head to minimize motion. To facilitate a waking state during the scan session, the subjects were allowed to watch a movie using an fMRI video projector.

Feasibility Study

In an initial sub-group of 8 subjects, we tested the feasibility of the proposed TRU-PC sequence and identified a protocol that can yield robust results in all subjects. Given the abundant and well-known venous structures in the mid-sagittal plane, we have focused the TRU-PC acquisition in this slice. The imaging parameters of our working protocol are as follows: single 2D slice, FOV=200×200 mm^2, Acquisition matrix = 276 (foot-to-head, readout direction) × 83 (anterior-to-posterior, phase-encoding direction), in-plane acquisition voxel size=0.72×2.41 mm^2, slice thickness = 5 mm, RT=668 ms, single k-line acquisition per TR, TE=4.9 ms, T2-preparation module used composite block pulses with a τ_{CPMG}=10ms and employed a MLEV-16 phase-cycling scheme; three effective TEs, 40 ms, 80 ms, 120ms, were used; scan duration= 7 minutes and 13 seconds. The value of V_{enc} should be chosen to be close to the flow velocity of the targeted vessel. For our experiment which aims to assess multiple vessels (i.e. various locations on the superior sagittal sinus,

straight sinus, great vein, internal cerebral vein) simultaneously, a pilot study was performed by using a range of V_{enc} values (80, 60, 40, 20, 15, 5 cm/s in the anterior-to-posterior direction) in a plain phase-contrast sequence and it was found that V_{enc}=15 cm/s provided the highest signal for most of the target vessels. This V_{enc} value was therefore used in all later experiments. It should be pointed out, however, that this is an empirical choice and the true optimal value could be subject-specific and vessel-specific. One can certainly use a "survey" phase-contrast scan to make refinement for each individual.

Validation Study

In a sub-group of 7 subjects, Y_v measured with TRU-PC was compared to a validated global Y_v technique, TRUST MRI (6), in the sagittal sinus. The optimized protocol and imaging parameters for TRUST MRI were used (34). Both TRU-PC and TRUST sequences were repeated multiple times to improve the measurement precision (which will be investigated in a later section). The TRUST technique can only measure Y_v in the posterior terminal of the superior sagittal sinus. Thus, the ROI selection for TRU-PC was chosen in the same region to facilitate the comparison. Comparison between results of the two methods was conducted using scatter plot, paired Student t test, and Pearson correlation coefficient. This allows the evaluation of measurement accuracy of TRU-PC when applied to the posterior superior sagittal sinus, although its accuracy in other locations is not assessed.

Vascular Reactivity Study

A sub-group of 5 subjects underwent a hypoxia maneuver to investigate the ability of TRU-PC in detecting the expected change in Y_v. The subjects breathed through a mouthpiece that was connected either to room air or to a bag containing 13% O_2 via a 3-way valve as described previously (35). TRU-PC MRI was performed before and during the breathing of 13% O_2, and subsequently compared. Vital signs including arterial oxygen saturation (Y_a), and end-tidal O_2 were recorded throughout the session.

Caffeine is known to modulate the venous blood oxygenation via blockage of adenosine receptors in the brain (36). We therefore studied an additional sub-group of 5 subjects using a caffeine challenge. The subjects were scanned before, and 1 hour after the ingestion of a 200 mg caffeine tablet (equivalent to two cups of regular coffee). During the 1 hour waiting period, the subjects were removed from the scanner, and repositioned after 50 minutes for the post-ingestion scan.

Reproducibility and EPI-acquisition Study

In an additional sub-group of 5 subjects, the reproducibility of TRU-PC was investigated while also testing the viability of reducing the scan duration. Three types of acquisition strategies were tested: the standard TRU-PC described above, a segmented-EPI acquisition with EPI-factor 3 (acquisition of 3 k-lines following each excitation), and a segmented-EPI acquisition with EPI-factor of 5. This set of scans was repeated four times during the session in an interleaved fashion. The imaging parameters for the multi-shot acquisitions were identical to the standard non-EPI TRU-PC, except for the following: (1) The scan with EPI-factor 3 used TE=6.7 ms, scan duration= 2 minutes and 24 seconds, (2) The scan with EPI-factor 5 used TE=7.7 ms, scan duration= 1 minute and 27 seconds. Reproducibility of each

acquisition strategy was evaluated by the intra-session coefficient of variation (CoV), defined as the standard deviation across repetitions divided by the mean (34). The Y_v values across different acquisition strategies were also compared to examine any systematic differences due to the EPI factor.

Feasibility of Small Vessel TRU-PC

We also wanted to extend the TRU-PC technique beyond the mid-sagittal major veins to evaluate oxygenation in smaller veins such as pial veins or deep veins. Thus, in a final subset of 6 subjects, we examined the feasibility of measuring the Y_v in small vessels. We first performed a Susceptibility-Weighted-Imaging (SWI) (37) to visualize veins in the slice of interest. The imaging parameters for SWI were: 3D gradient echo readout, read-out BW=80Hz, FOV=230×164mm2, matrix=480×480, 48 slices, slice thickness = 2mm, slice gap = 0mm, TR=40ms, TE=25ms, FA=20°, scan duration=4.3 min. Then, TRU-PC was performed to estimate the blood oxygenation of the targeted veins. Given that the smaller vessels have smaller size and lower flow velocity, we made two adjustments to our protocol: voxel size in the phase-encoding direction was reduced from 2.4 mm to 1.2mm; V_{enc} was reduced from 15 cm/s to 5 cm/s. These changes resulted in an increase in scan duration to 14 minutes and 20 seconds (no EPI was applied in these scans yet). Both axial and sagittal acquisition planes were evaluated.

Data Analysis

The data was processed with in-house MATLAB (Mathworks, Natick, MA) scripts. Motion correction between the three eTE images was performed with the software FSL (University of Oxford, UK). Before the data was fit for T_2, the noise level of each image was determined by manually drawing a region-of-interest (ROI) in the static tissue region (e.g. green boxes in Figure 2). The noise level was computed according to the Rayleigh noise equation (38):

$$\sigma_{noise} = \frac{\text{mean}\,(S_{noise})}{\sqrt{\pi/2}}. \quad [4]$$

The Rayleigh noise can skew the distribution of the signals in the image, forcing it to a non-Gaussian function. This is particularly relevant for low intensity signals (e.g. the signal of long eTE), and should be corrected. The signal correction followed a standard method (39):

$$S_{corrected} = \sqrt{|S_{blood}^2 - \sigma_{noise}^2|}. \quad [5]$$

The corrected blood signal was then fit to a mono-exponential function of eTE to obtain $T_{2,blood}$ (c.f. Eq. [3]). The fitting was performed on a voxel-by-voxel level as well as on ROIs. For ROI analysis, a preliminary mask was manually placed on the eTE 40 image (typically containing about 200 voxels) and the top 100 voxels by signal intensity were included in the final mask. The mono-exponential fitting for the ROI data was conducted such that each voxel in the ROI was allowed to have independent signal intensity, S_0, but with the constraint of a common $T_{2,blood}$. By assuming Hct=41% for all subjects, the blood T_2 was converted to Y_v using a previously established calibration plot (40). For the small

vessel data, only ROI analysis was performed. The venous vessel was first identified on the SWI image and a preliminary mask on the eTE-40 TRU-PC image was drawn to encompass this vessel. A visual inspection on all eTE images, in particular eTE of 120ms, was conducted to ensure that the vessel signal is clearly above background noise before the fitting was carried out. This step of visual inspection was not needed for the large vessel data as their signals were clearly above noise.

Results

Feasibility Study

TRU-PC MRI results in three types of images: a complex average (CA) image between the "+" and "−" scans, a complex difference (CD) image, and a velocity image based on phase differences between the "+" and "−" scans. Figure 2a shows the three types of images at each eTE. The CA image contains both tissue and blood signal with discernible anatomical structures, and decays appreciably with increasing T_2 weighting. The CD images also decay with eTE. Importantly, the decay rate in CD is only dependent on the T_2 of blood, but not tissue, due to the isolation of pure blood signal. Note that the pulsation of arterial vessels did not yield a clear ghosting in this sequence. This is because the TR is relatively long and there is not a simple pattern of cardiac-phase-related periodicity in the k space data. The velocity images do not depend on eTE as it is related to the phase, not magnitude, of the magnetization. Note, however, that the velocity image is susceptible to tissue partial voluming, unlike the CD image.

A sample decay of the CD signal as a function of eTE is shown in Figure 2b. The resulting T_2 was extracted using a monoexponential model, and converted to Y_v using a calibration curve measured previously using identical T_2-preparation pulses (40) (Figure 3c).

The ROI can be drawn on any of the vessels seen in the CD image. For quantification in this study, we defined 8 main vascular regions based on a brain vein atlas (41). Figure 3a shows the chosen ROIs, where the Superior Sagittal Sinus (SSS) has been partitioned into five sections (denoted as ROI #1–5, respectively), and the remaining ROIs are centered on the Straight Sinus (SS, ROI #6), Great Vein (GV, ROI #7), and Internal Cerebral Vein (ICV, ROI #8). In this designation scheme, ROIs #1–5 drain the cortex and ROIs #6–8 drain the deep brain regions. The path of the venous flow is also labeled in Figure 3c.

Figure 3c shows group-averaged Y_v values for each ROI (N=22 including 7 subjects from validation study, 5 subjects from O2 study's baseline scan, 5 subjects from caffeine study's baseline scan, 5 from reproducibility study). Comparison across ROIs was only carried out for consecutive regions due to their physical adjacency. Significant differences were observed in four neighboring ROI pairs (paired t test, Bonferroni-corrected $P<0.05$) (see Figure 3c). The Y_v difference between ROI #5 and 6 have been reported previously by Jain et al (42).

Figure 3b shows a map of Y_v based on voxel-wise T_2 fitting (only voxels with CD intensity > 4 times the noise level were used). It is apparent that the T_2 fitting is stable across the entire path of the venous structure. Interestingly, the mid-sagittal slice also includes a

feeding artery, i.e. basilar artery, and Y_v in the artery was found to be close to 100% (Figure 3b), as expected.

Validation Study

Y_v values measured with TRU-PC were compared to Y_v determined by TRUST MRI. ROI #4 was used for the comparison because it is the location that the TRUST measure is based upon. The average TRU-PC Y_v value of 61.3 ± 6.7% (mean ± SD, N=7) showed no difference (P=0.90) from the TRUST average Y_v of 61.4 ± 8.3%. Figure 4 shows the scatter plot between the TRU-PC and TRUST measured Y_v values. A linear relationship close to the unit line was observed between them (N=7, P=0.001).

Vascular Reactivity Study

To test if TRU-PC could detect a change in blood oxygen saturation, two physiologic challenge experiments were performed. In a subgroup of five subjects, a hypoxia maneuver was performed. A summary of the fraction of inhaled oxygen (FiO_2), end-tidal O_2 (EtO_2), and Y_a during the normoxic and hypoxic conditions are listed in Table 1. Y_v values in the 8 ROIs are plotted in Figure 5a. Y_v during hypoxia was lower than that during normoxia in all ROIs, consistent with the expected effects of this type of challenge. The average decrease in Y_v was 6.6 ± 3.8%.

Furthermore, a caffeine challenge was tested on 5 subjects. Caffeine is known to reduce cerebral blood flow and venous oxygenation (36). Figure 5b shows Y_v in the 8 ROIs evaluated by TRU-PC. A decrease in Y_v was observed in all ROIs with an average reduction of 9.1 ± 2.6%.

Reproducibility and EPI-acquisition Study

Reproducibility of the TRU-PC technique was evaluated by performing four repetitions in the same session with a 12-minute interval between measures (N=5). The coefficient of variation (CoV) averaged over all ROIs was 3.5 ± 1.0%, which is larger than the TRUST CoV of 1.9 ± 0.6% as reported in the literature (34), but can still be considered acceptable. Figure 6a (blue curve) shows CoV of individual ROI.

Given that all TRU-PC data presented so far were acquired with a relatively long scan duration of 7.2 minutes, we also tested the feasibility of segmented-EPI acquisition to reduce the scan duration. A representative map of Y_v acquired with non-EPI, EPI-factor 3 (scan duration 2.4 min), and EPI-factor 5 (scan duration 1.5 min) is shown in Figure 6b. Quantitative comparison of CoV across the three acquisition strategies is shown in Figure 6a (N=5). It appears that the use of segmented-EPI did not significantly impact the reproducibility of the measures. The values of Y_v measured with the three strategies were also comparable, and no significant difference was identified. Thus, segmented EPI may provide a rapid method for TRU-PC acquisition.

Feasibility of Small Vessel TRU-PC

We measured Y_v in smaller veins (1–2 mm in diameter as determined from SWI images) in six subjects. The cut-off velocity and spatial resolution were adjusted accordingly as

described in Methods. In three subjects, we applied a sagittal planning to measure pial veins that drain cortical gray matter. Figure 7 shows results from individual subjects. CD images from TRU-PC are displayed as a function of eTE. Y_v values of representative veins are also displayed (note: these veins do not have designated names). In another three subjects, we applied an axial planning to measure Y_v of deep veins that drain deep gray matter (e.g. basal ganglia, thalamus). The resulting TRU-PC images and the corresponding oxygen saturations are shown in Figure 8.

Discussion

This study presented a novel TRU-PC MRI technique that uses completely non-invasive procedures and a relatively simple analysis method to quantify blood oxygenation in cerebral veins. We have demonstrated that this technique is capable of measuring oxygenation in major cerebral veins as well as pial and deep veins. The accuracy of TRU-PC was verified by showing an excellent agreement with a validated global method, TRUST MRI. The technique was also found to be highly reproducible with a CoV of 3.5% among repeated measures. Finally, using two separate physiologic challenges, the sensitivity of TRU-PC MRI in detecting changes in oxygenation was demonstrated.

Clinical potentials

The brain represents about 2% of the total body weight, but consumes about 20% of the total energy. Therefore, the rate of energy utilization and oxygen consumption is an important index of tissue viability and brain function. Abnormal levels of oxygen metabolism have been documented in vascular dementia (43), multiple sclerosis (MS) (22,44,45), brain tumors (46), head injury (47,48), and a variety of metabolic disorders (e.g. diabetes) (49–52). It is well known that the cerebral metabolic rate of oxygen ($CMRO_2$) can be quantified by the arterio-venous difference in oxygen content (53). However, while the arterial oxygenation can be measured easily from the periphery (since all arterial blood comes from the heart and has the same oxygenation), the venous oxygenation must be measured in the brain itself and has presented major technical challenges. Therefore, the development of TRU-PC MRI to quantify venous oxygenation could potentially fill this gap and make it feasible to measure $CMRO_2$ on a routine basis.

It should also be noted that recent advances in MRI technologies have allowed measurement of *global* venous oxygenation. An example of such a method is the TRUST MRI technique that our group has previously developed (6). We, however, emphasize that a regional oxygenation and $CMRO_2$ technique will have additional important clinical applications. First, a better characterization of variations in venous oxygenation across brain regions may improve our understanding of spatial patterns of oxygen extraction reserve and allow the identification of regions with greater risk for ischemia attack or stroke. Second, the ability to measure oxygenation in a specific vein may be used in task-activation studies to understand physiology during brain activation, which is usually region-specific. Third, many brain disorders are known to affect a specific brain region, thus venous oxygenation measurement of the whole-brain may not be able to detect the abnormality. In particular, knowledge of oxygenation and metabolism in the deep gray matter (e.g. basal ganglia, thalamus) has

unique significance in understanding pathophysiology of several diseases including Parkinson's disease in which dopaminergic neurons in basal ganglia suffer from increased cell death (54), Huntington's disease in which caudate and putamen are particularly vulnerable to the toxic mHtt protein (55), and Wilson's disease in which the abnormal metal ion accumulation is especially pronounced in subcortical nuclei (56). Using ^{15}O-PET, Wolfson and colleagues demonstrated an elevated oxygen extraction fraction (OEF) in Parkinsonism, which would correspond to a reduction in venous oxygenation (57). Evaluating glucose metabolism, a number of researchers have shown that patients with Parkinson's disease have a greater metabolic rate in the deep brain regions when compared to healthy controls, whereas the patients' cortical metabolic rate was suppressed (58). In Huntington's disease, the basal ganglia showed a decrease in metabolism whereas the thalamus showed an increase (58). In Wilson's disease, Kuwert and colleagues found that thalamic glucose metabolism was significantly lower than that in control subjects (59). Therefore, the ability of TRU-PC to measure deep vein oxygenation may find immediate applications in these clinical conditions.

Comparison with other techniques

The PET method is the current gold-standard for Y_v and $CMRO_2$ measurements. It uses three radiolabel tracers, $H_2{}^{15}O$, $C^{15}O$, $^{15}O_2$, and a kinetic model to estimate the parameters. However, since these tracers have a very short half-life (about 2 minutes), these measurements require an onsite cyclotron at the imaging facility, equipment that is available to only approximately 10% of the PET facilities in the United States. Additionally, the procedures associated with the use of three different tracers are rather complex and, furthermore, an arterial line is needed during the imaging session to sample the arterial input function. For these reasons, the PET Y_v measurement has not been routinely used in clinical or research practice. For MRI methods, the qBOLD technique uses a MR signal model accounting for multiple tissue compartments and hemodynamic parameters such as blood volume and venous oxygenation, and performs model fitting to estimate Y_v (9). A potential limitation of this method is the complexity of the model and its high sensitivity to magnetic field inhomogeneity (e.g. quality of shimming). The PROM method (15) uses a susceptibility phase difference between the venous blood and the surrounding tissue to quantify Y_v. But this technique requires assumptions on vessel orientation, is sensitive to field inhomogeneity, and requires the selection of a reference tissue (which is not always trivial). Two newer techniques, QUXOTIC (23) and VSEAN (24), use velocity-selective spin tagging to isolate pure blood signal and estimate blood T_2, and have shown promising preliminary data. However, reproducibility of these two techniques has not been fully evaluated and there remain several technical issues related to the potential contributions from capillary/CSF/static tissue as well as the hematocrit differences between microvascular and macrovascular vessels, which can affect the T_2-oxygenation relationship. Two recent studies have also proposed to use concomitant hypercapnia and hyperoxia challenges to estimate Y_v (60,61). The practicality of the challenges and the validity of certain assumptions require further verification.

The TRU-PC technique proposed in this study uses a simple data processing approach of mono-exponential fitting with few assumptions, since the theoretical framework of the

method is relatively straightforward. The technique also does not require the selection of a reference tissue. Signals in TRU-PC are expected to have minimal, if any, contributions from CSF or capillary signal due to the large V_{enc} used. Furthermore, uncertainty in the hematocrit value is not an issue since the blood signal is of macrovascular origin.

Our method is also in contrast to the technique developed by Jain et al (42), which is a global measure and devoid of spatial information. Their method, however, possesses the clear advantage of high temporal resolution (~30 sec) that TRU-PC lacks.

The use of flow-selective magnetization preparation within a T_2 module has previously been used in angiogram studies for suppression of large-vessel signals (62–66). The sequence design rationale was, however, different from that of the present study in that the previous studies used T_2 preparation as a “wrapper” to embed the flow-suppressing gradients, rather than for the purpose of modulating the T_2 weighting as used in the present design. In fact, the T_2 decay in the previous studies was an undesired effect. Additionally, the T_2 preparation and flow-encoding were applied in different sequence modules in our study, whereas they were applied in the same module in the earlier studies. Furthermore, our sequence used varying T_2 weightings and provides an estimation of T_2 value, which the previous sequence did not measure (65,66). Finally, our sequence used a CPMG-T2-prep rather than the spin-echo T2-prep used in the previous literature (65,66). Compared to spin-echo T_2, CPMG-T_2 is less sensitive to macroscopic field inhomogeneity due to shimming imperfection and is more widely used in studies of blood oxygenation estimation (6,18,23).

The present study observed that venous oxygenation across major vessel branches is within the general range of 50–75%, consistent with previous reports (67). However, we also observed that the deep veins have a slightly higher Y_v compared to cortical veins (Figure 3). This finding is in agreement with previous literature that deep brain tends to have a lower oxygen extraction fraction (OEF) (Note that OEF=1−Y_v) (68–71). Within the cortical venous path, the anterior locations tend to have a greater Y_v compared to posterior locations (Figure 3). This is consistent with PET findings that OEF is lower in frontal cortex compared to parietal cortex, which is again lower than occipital cortex (68). Similar profile was observed in the deep vein path in our data. This could be because the beginning segments of the deep veins (ROI #8 internal cerebral vein and ROI #7 great vein) primarily drain deep gray matter which has lower OEF as described above, whereas the later segment (ROI #6, straight sinus) also contains blood from the inferior sagittal sinus which drains cortical tissue. The reason for a lower OEF in deep gray matter appears to be related to greater blood flow to these regions, as shown by previous PET results (68).

Technical considerations

Scan duration is an important factor in evaluating the practicality of a technique. The proof-of-principle scans performed in the present study used a conservative acquisition approach of non-EPI gradient-echo, which resulted in a relatively long scan duration of 7.2 minutes. We later employed segmented-EPI acquisition with an EPI factor of 5, allowing us to reduce the time to 1.5 minutes. This duration is more desirable for future clinical applications. The reproducibility data of the segmented-EPI sequences further showed that the use of EPI did not negatively impact the reliability of the results. Although it is expected that segmented-

EPI would result in lower SNR compared to conventional gradient-echo acquisition (due to T2* decay), the shortening of scan duration may have reduced the motion-related noise in the data. Thus, the overall data stability is comparable.

In the TRU-PC sequence, we included a non-slice-selective post-saturation to reset the magnetization of all spins to zero. Since the TRU-PC technique measures flowing spins, it is conceivable that different spins may have experienced a different number of RF pulses during previous periods. For example, spins traveling through the imaging slice will have experienced all of the T_2-preparation and excitation pulses, whereas fresh blood spins entering the brain may not have experienced any RF pulses. Therefore, the use of a global post-saturation pulse ensures that all spins follow the saturation recovery evolution as modeled by the theory.

Conventional phase-contrast MRI usually uses a smaller flip angle (e.g. 15°) and a shorter TR, which is helpful in reducing scan duration. In TRU-PC MRI, regardless of the flip angle of the excitation pulse, the magnetization needs to recover from zero (after the post-saturation pulse). Thus, an excitation flip angle of 90° is used to maximize the signal. For similar reasons, a relatively long RT (668ms) is needed to allow sufficient recovery of the longitudinal magnetization. The minimal TR is also constrained by the SAR of the sequence.

The T_2-preparation of the TRU-PC sequence used three different eTE values: 40 ms, 80 ms, and 120 ms. Given that our τ_{CPMG}=10 ms, this corresponded to 4, 8 and 12 refocusing pulses. Since we are using MLEV-16 phase cycling on the composite pulses of the T_2-preparation, a multiple of 4 refocusing pulses can minimize the effect of RF imperfection (72). We did not include an eTE of zero (i.e. tip down and immediately tip up) in our TRU-PC acquisition because the phase of the transverse magnetization may change slightly between tip-down and tip-up, resulting in imperfect tip-up and the under-estimation of signal at eTE 0 ms. This effect can be sizable in regions where resonance offset (i.e. field inhomogeneity) is severe.

Limitations

One of the limitations is that the TRU-PC technique as presented can only measure oxygenation in macrovessels but not microvessels. In other words, at present TRU-PC can only study veins that one can visualize in an anatomic (e.g. SWI in Figure 7) image. Based on our data, these veins typically have a diameter of 1 mm or above. For veins smaller than this caliber, the sensitivity of the signal will be questionable. In addition, if the voxel contains two or more small vessels, their phase-contrast CD signals may cancel out instead of summing up. The ability of TRU-PC in quantifying microvascular Y_v is further complicated by the fact that hematocrit is known to progressively decrease in microvessels (73). Since hematocrit can significantly modulate the blood T_2-Y relationship, this uncertainty is expected to compromise the accuracy of the estimation, a limitation suffered by all T_2-based regional Y_v techniques.

Conclusion

We presented a novel technique, TRU-PC MRI, to non-invasively quantify cerebral oxygenation in regional draining veins with a diameter of 1 mm or greater. Methodological evaluations revealed that this technique is accurate when compared to established approaches, is reproducible, and has sufficient sensitivity in detecting oxygenation changes due to typical physiologic challenges. Thus, this simple technique may provide a critical step toward region-specific measurement of oxygenation and metabolism in the brain.

Acknowledgments

Grant Sponsors: NIH R01 MH084021, NIH R01 NS067015, NIH R01 AG042753, NIH R21 NS078656, NIH R01 NS076588, National MS Society RG 4707A1

References

1. Diringer MN, Aiyagari V, Zazulia AR, Videen TO, Powers WJ. Effect of hyperoxia on cerebral metabolic rate for oxygen measured using positron emission tomography in patients with acute severe head injury. J Neurosurg. 2007; 106(4):526–529. [PubMed: 17432700]
2. Kudomi N, Hayashi T, Teramoto N, Watabe H, Kawachi N, Ohta Y, Kim KM, Iida H. Rapid quantitative measurement of CMRO(2) and CBF by dual administration of (15)O-labeled oxygen and water during a single PET scan-a validation study and error analysis in anesthetized monkeys. J Cereb Blood Flow Metab. 2005; 25(9):1209–1224. [PubMed: 15874976]
3. Mintun M, Raichle M, Martin W, Herscovitsch P. Brain oxygen utilization measured with O-15 radiotracers and positron emission tomography. J Nucl Med. 1984; 25:118–126.
4. Fernandez-Seara MA, Techawiboonwong A, Detre JA, Wehrli FW. MR susceptometry for measuring global brain oxygen extraction. Magn Reson Med. 2006; 55(5):967–973. [PubMed: 16598726]
5. Jain V, Langham MC, Wehrli FW. MRI estimation of global brain oxygen consumption rate. J Cereb Blood Flow Metab. 2010; 30(9):1598–1607. [PubMed: 20407465]
6. Lu H, Ge Y. Quantitative evaluation of oxygenation in venous vessels using T2-Relaxation-Under-Spin-Tagging MRI. Magn Reson Med. 2008; 60(2):357–363. [PubMed: 18666116]
7. Lu H, Zhao C, Ge Y, Lewis-Amezcua K. Baseline blood oxygenation modulates response amplitude: Physiologic basis for intersubject variations in functional MRI signals. Magn Reson Med. 2008; 60(2):364–372. [PubMed: 18666103]
8. Bulte DP, Kelly M, Germuska M, Xie J, Chappell MA, Okell TW, Bright MG, Jezzard P. Quantitative measurement of cerebral physiology using respiratory-calibrated MRI. Neuroimage. 2012; 60(1):582–591. [PubMed: 22209811]
9. Christen T, Lemasson B, Pannetier N, Farion R, Segebarth C, Remy C, Barbier EL. Evaluation of a quantitative blood oxygenation level-dependent (qBOLD) approach to map local blood oxygen saturation. NMR Biomed. 2010; 24(4):393–403. [PubMed: 20960585]
10. Yablonskiy DA, Haacke EM. Theory of NMR signal behavior in magnetically inhomogeneous tissues: the static dephasing regime. Magn Reson Med. 1994; 32(6):749–763. [PubMed: 7869897]
11. An H, Lin W. Quantitative measurements of cerebral blood oxygen saturation using magnetic resonance imaging. J Cereb Blood Flow Metab. 2000; 20(8):1225–1236. [PubMed: 10950383]
12. He X, Yablonskiy DA. Quantitative BOLD: mapping of human cerebral deoxygenated blood volume and oxygen extraction fraction: default state. Magn Reson Med. 2007; 57(1):115–126. [PubMed: 17191227]
13. He X, Zhu M, Yablonskiy DA. Validation of oxygen extraction fraction measurement by qBOLD technique. Magn Reson Med. 2008; 60(4):882–888. [PubMed: 18816808]
14. Haacke EM, Lai S, Reichenbach JR, Kuppusamy K, Hoogenraad FG, Takeichi H, Lin W. In vivo measurement of blood oxygen saturation using magnetic resonance imaging: a direct validation of

the blood oxygen level-dependent concept in functional brain imaging. Hum Brain Mapp. 1997; 5(5):341–346. [PubMed: 20408238]

15. Fan AP, Benner T, Bolar DS, Rosen BR, Adalsteinsson E. Phase-based regional oxygen metabolism (PROM) using MRI. Magn Reson Med. 2012; 67(3):669–678. [PubMed: 21713981]
16. Liu J, Liu T, de Rochefort L, Ledoux J, Khalidov I, Chen W, Tsiouris AJ, Wisnieff C, Spincemaille P, Prince MR, Wang Y. Morphology enabled dipole inversion for quantitative susceptibility mapping using structural consistency between the magnitude image and the susceptibility map. Neuroimage. 2012; 59(3):2560–2568. [PubMed: 21925276]
17. Liu T, Spincemaille P, de Rochefort L, Kressler B, Wang Y. Calculation of susceptibility through multiple orientation sampling (COSMOS): a method for conditioning the inverse problem from measured magnetic field map to susceptibility source image in MRI. Magn Reson Med. 2009; 61(1):196–204. [PubMed: 19097205]
18. Golay X, Silvennoinen MJ, Zhou J, Clingman CS, Kauppinen RA, Pekar JJ, van Zij PC. Measurement of tissue oxygen extraction ratios from venous blood T(2): increased precision and validation of principle. Magn Reson Med. 2001; 46(2):282–291. [PubMed: 11477631]
19. Oja JM, Gillen J, Kauppinen RA, Kraut M, van Zijl PC. Venous blood effects in spin-echo fMRI of human brain. Magn Reson Med. 1999; 42(4):617–626. [PubMed: 10502748]
20. Wright GA, Hu BS, Macovski A. 1991 I.I. Rabi Award. Estimating oxygen saturation of blood in vivo with MR imaging at 1. 5 T. J Magn Reson Imaging. 1991; 1(3):275–283. [PubMed: 1802140]
21. Wong EC, Buxton RB, Frank LR. Implementation of quantitative perfusion imaging techniques for functional brain mapping using pulsed arterial spin labeling. NMR Biomed. 1997; 10(4–5):237–249. [PubMed: 9430354]
22. Ge Y, Zhang Z, Lu H, Tang L, Jaggi H, Herbert J, Babb JS, Rusinek H, Grossman RI. Characterizing brain oxygen metabolism in patients with multiple sclerosis with T2-relaxation-under-spin-tagging MRI. J Cereb Blood Flow Metab. 2011; 32(3):403–412. [PubMed: 22252237]
23. Bolar DS, Rosen BR, Sorensen AG, Adalsteinsson E. QUantitative Imaging of eXtraction of oxygen and TIssue consumption (QUIXOTIC) using venular-targeted velocity-selective spin labeling. Magn Reson Med. 2011; 66(6):1550–1562. [PubMed: 21674615]
24. Guo J, Wong EC. Venous oxygenation mapping using velocity-selective excitation and arterial nulling. Magn Reson Med. 2012; 68(5):1458–1471. [PubMed: 22294414]
25. Krishnamurthy, L.; Liu, P.; Lu, H. Vessel-specific measurement of blood oxygenation with T2-Relaxation-Under-Phase-Contrast (TRU-PC) MRI. Gordon Resaerch Conference: In-vivo Magnetic Resonance; Waterville, Maine. 2012. p. 13
26. Bernstein MA, Ikezaki Y. Comparison of phase-difference and complex-difference processing in phase-contrast MR angiography. J Magn Reson Imaging. 1991; 1(6):725–729. [PubMed: 1823179]
27. Bernstein, MA.; King, KF.; Zhou, XJ. Phase Contrast: Handbook of MRI Pulse Sequences. Burlington, MA: Elsevier Academic Press; 2004.
28. Haacke, ME.; Brown, RW.; Thompson, MR.; Venkatesan, R. Magnetic Resonance Imaging: Physical Principles and Sequence Design. New York, NY: Wiley-Liss; 1999. MR Angiography and Flow Quantification.
29. Polzin JA, Alley MT, Korosec FR, Grist TM, Wang Y, Mistretta CA. A complex-difference phase-contrast technique for measurement of volume flow rates. J Magn Reson Imaging. 1995; 5(2):129–137. [PubMed: 7766973]
30. Lu, H. Magnetization “Reset” for Non-Steady-State Blood Spins in Vascular-Space-Occupancy (VASO) fMRI. Proceedings of the International Society for Magnetic Resonance in Medicine; Toronto, Canada. 2008. p. 406
31. Pell GS, Thomas DL, Lythgoe MF, Calamante F, Howseman AM, Gadian DG, Ordidge RJ. Implementation of quantitative FAIR perfusion imaging with a short repetition time in time-course studies. Magn Reson Med. 1999; 41(4):829–840. [PubMed: 10332861]
32. Xu F, Uh J, Liu P, Lu H. On improving the speed and reliability of T2-relaxation-under-spin-tagging (TRUST) MRI. Magn Reson Med. 2011; 68(1):198–204. [PubMed: 22127845]

33. Wu WC, Buxton RB, Wong EC. Vascular space occupancy weighted imaging with control of residual blood signal and higher contrast-to-noise ratio. IEEE Trans Med Imaging. 2007; 26(10): 1319–1327. [PubMed: 17948723]
34. Liu P, Xu F, Lu H. Test-retest reproducibility of a rapid method to measure brain oxygen metabolism. Magn Reson Med. in press. 10.1002/mrm.24295
35. Xu F, Liu P, Pascual JM, Xiao G, Lu H. Effect of hypoxia and hyperoxia on cerebral blood flow, blood oxygenation, and oxidative metabolism. J Cereb Blood Flow Metab. 2012; 32:1909–1918. [PubMed: 22739621]
36. Mulderink TA, Gitelman DR, Mesulam MM, Parrish TB. On the use of caffeine as a contrast booster for BOLD fMRI studies. Neuroimage. 2002; 15(1):37–44. [PubMed: 11771972]
37. Haacke EM, Xu Y, Cheng YC, Reichenbach JR. Susceptibility weighted imaging (SWI). Magn Reson Med. 2004; 52(3):612–618. [PubMed: 15334582]
38. Papoulis, A. Probability, Random Variables, and Stochastic Processes. New York, NY: McGraw Hill, Inc; 1991.
39. Gudbjartsson H, Patz S. The Rician distribution of noisy MRI data. Magn Reson Med. 1995; 34(6): 910–914. [PubMed: 8598820]
40. Lu H, Xu F, Grgac K, Liu P, Qin Q, van Zijl P. Calibration and validation of TRUST MRI for the estimation of cerebral blood oxygenation. Magn Reson Med. 2012; 67(1):42–49. [PubMed: 21590721]
41. Moore, KL.; Dalley, AF. Clinically Oriented Anatomy. Philadelphia, PA: Lippincott Williams & Wilkins; 1999.
42. Jain, V.; Magland, J.; Langham, MC.; Wehrli, FW. High Temporal Resolution In-Vivo Blood Oximetry via Projection Based T2 Measurement. Proceedings of International Society for Magnetic Resonance in Medicine; Melbourne, Austrlia. 2012. p. 2184
43. Yao H, Sadoshima S, Ibayashi S, Kuwabara Y, Ichiya Y, Fujishima M. Leukoaraiosis and dementia in hypertensive patients. Stroke. 1992; 23(11):1673–1677. [PubMed: 1440720]
44. Paling D, Golay X, Wheeler-Kingshott C, Kapoor R, Miller D. Energy failure in multiple sclerosis and its investigation using MR techniques. J Neurol. 2011; 258(12):2113–2127. [PubMed: 21660561]
45. Sun X, Tanaka M, Kondo S, Okamoto K, Hirai S. Clinical significance of reduced cerebral metabolism in multiple sclerosis: a combined PET and MRI study. Ann Nucl Med. 1998; 12(2): 89–94. [PubMed: 9637279]
46. Leenders KL. PET: blood flow and oxygen consumption in brain tumors. J Neurooncol. 1994; 22(3):269–273. [PubMed: 7760106]
47. Glenn TC, Kelly DF, Boscardin WJ, McArthur DL, Vespa P, Oertel M, Hovda DA, Bergsneider M, Hillered L, Martin NA. Energy dysfunction as a predictor of outcome after moderate or severe head injury: indices of oxygen, glucose, and lactate metabolism. J Cereb Blood Flow Metab. 2003; 23(10):1239–1250. [PubMed: 14526234]
48. Grant PE, Roche-Labarbe N, Surova A, Themelis G, Selb J, Warren EK, Krishnamoorthy KS, Boas DA, Franceschini MA. Increased cerebral blood volume and oxygen consumption in neonatal brain injury. J Cereb Blood Flow Metab. 2009; 29(10):1704–1713. [PubMed: 19675563]
49. Miyajima H, Takahashi Y, Kono S. Aceruloplasminemia, an inherited disorder of iron metabolism. Biometals. 2003; 16(1):205–213. [PubMed: 12572680]
50. Shishido F, Uemura K, Inugami A, Tomura N, Higano S, Fujita H, Sasaki H, Kanno I, Murakami M, Watahiki Y, Nagata K. Cerebral oxygen and glucose metabolism and blood flow in mitochondrial encephalomyopathy: a PET study. Neuroradiology. 1996; 38(2):102–107. [PubMed: 8692416]
51. Sieber FE, Brown PR, Wu Y, Koehler RC, Traystman RJ. Cerebral blood flow and metabolism in dogs with chronic diabetes. Anesthesiology. 1993; 79(5):1013–1021. [PubMed: 8238980]
52. Uchino K, Lin R, Zaidi SF, Kuwabara H, Sashin D, Bircher N, Chang YF, Hammer MD, Reddy V, Jovin TG, Vora N, Jumaa M, Massaro L, Billigen J, Boada F, Yonas H, Nemoto EM. Increased Cerebral Oxygen Metabolism and Ischemic Stress in Subjects with Metabolic Syndrome-Associated Risk Factors: Preliminary Observations. Transl Stroke Res. 2010; 1(3):178–183. [PubMed: 22034586]

53. Xu F, Ge Y, Lu H. Noninvasive quantification of whole-brain cerebral metabolic rate of oxygen (CMRO2) by MRI. Magn Reson Med. 2009; 62(1):141–148. [PubMed: 19353674]
54. Obeso JA, Rodriguez-Oroz MC, Benitez-Temino B, Blesa FJ, Guridi J, Marin C, Rodriguez M. Functional organization of the basal ganglia: therapeutic implications for Parkinson's disease. Mov Disord. 2008; 23 (Suppl 3):S548–559. [PubMed: 18781672]
55. Walker FO. Huntington's disease. Lancet. 2007; 369(9557):218–228. [PubMed: 17240289]
56. Lorincz MT. Neurologic Wilson's disease. Ann N Y Acad Sci. 2010; 1184:173–187. [PubMed: 20146697]
57. Wolfson LI, Leenders KL, Brown LL, Jones T. Alterations of regional cerebral blood flow and oxygen metabolism in Parkinson's disease. Neurology. 1985; 35(10):1399–1405. [PubMed: 4033924]
58. Ma Y, Eidelberg D. Functional imaging of cerebral blood flow and glucose metabolism in Parkinson's disease and Huntington's disease. Mol Imaging Biol. 2007; 9(4):223–233. [PubMed: 17334854]
59. Kuwert T, Hefter H, Scholz D, Milz M, Weiss P, Arendt G, Herzog H, Loken M, Hennerici M, Feinendegen LE. Regional cerebral glucose consumption measured by positron emission tomography in patients with Wilson's disease. Eur J Nucl Med. 1992; 19(2):96–101. [PubMed: 1563446]
60. Gauthier CJ, Hoge RD. Magnetic resonance imaging of resting OEF and CMRO(2) using a generalized calibration model for hypercapnia and hyperoxia. Neuroimage. 2011; 60(2):1212–1225. [PubMed: 22227047]
61. Gauthier CJ, Hoge RD. A generalized procedure for calibrated MRI incorporating hyperoxia and hypercapnia. Hum Brain Mapp. in press. 10.1002/hbm.21495
62. Sirol M, Itskovich VV, Mani V, Aguinaldo JG, Fallon JT, Misselwitz B, Weinmann HJ, Fuster V, Toussaint JF, Fayad ZA. Lipid-rich atherosclerotic plaques detected by gadofluorine-enhanced in vivo magnetic resonance imaging. Circulation. 2004; 109(23):2890–2896. [PubMed: 15184290]
63. Pell GS, Lewis DP, Branch CA. Pulsed arterial spin labeling using TurboFLASH with suppression of intravascular signal. Magn Reson Med. 2003; 49(2):341–350. [PubMed: 12541255]
64. Ye FQ, Mattay VS, Jezzard P, Frank JA, Weinberger DR, McLaughlin AC. Correction for vascular artifacts in cerebral blood flow values measured by using arterial spin tagging techniques. Magn Reson Med. 1997; 37(2):226–235. [PubMed: 9001147]
65. Fan Z, Sheehan J, Bi X, Liu X, Carr J, Li D. 3D noncontrast MR angiography of the distal lower extremities using flow-sensitive dephasing (FSD)-prepared balanced SSFP. Magn Reson Med. 2009; 62(6):1523–1532. [PubMed: 19877278]
66. Nguyen TD, de Rochefort L, Spincemaille P, Cham MD, Weinsaft JW, Prince MR, Wang Y. Effective motion-sensitizing magnetization preparation for black blood magnetic resonance imaging of the heart. J Magn Reson Imaging. 2008; 28(5):1092–1100. [PubMed: 18972350]
67. Coles JP, Minhas PS, Fryer TD, Smielewski P, Aigbirihio F, Donovan T, Downey SP, Williams G, Chatfield D, Matthews JC, Gupta AK, Carpenter TA, Clark JC, Pickard JD, Menon DK. Effect of hyperventilation on cerebral blood flow in traumatic head injury: clinical relevance and monitoring correlates. Crit Care Med. 2002; 30(9):1950–1959. [PubMed: 12352026]
68. Perlmutter JS, Powers WJ, Herscovitch P, Fox PT, Raichle ME. Regional asymmetries of cerebral blood flow, blood volume, and oxygen utilization and extraction in normal subjects. J Cereb Blood Flow Metab. 1987; 7(1):64–67. [PubMed: 3492507]
69. Hatazawa J, Fujita H, Kanno I, Satoh T, Iida H, Miura S, Murakami M, Okudera T, Inugami A, Ogawa T, et al. Regional cerebral blood flow, blood volume, oxygen extraction fraction, and oxygen utilization rate in normal volunteers measured by the autoradiographic technique and the single breath inhalation method. Ann Nucl Med. 1995; 9(1):15–21. [PubMed: 7779525]
70. Nakane H, Ibayashi S, Fujii K, Sadoshima S, Irie K, Kitazono T, Fujishima M. Cerebral blood flow and metabolism in patients with silent brain infarction: occult misery perfusion in the cerebral cortex. J Neurol Neurosurg Psychiatry. 1998; 65(3):317–321. [PubMed: 9728942]
71. Ibaraki M, Miura S, Shimosegawa E, Sugawara S, Mizuta T, Ishikawa A, Amano M. Quantification of cerebral blood flow and oxygen metabolism with 3-dimensional PET and 15O:

validation by comparison with 2-dimensional PET. J Nucl Med. 2008; 49(1):50–59. [PubMed: 18077532]

72. Levitt MH, Freeman R, Frenkiel T. Broadband Heteronuclear Decoupling. J Magnetic Res. 1982; 47:328–330.
73. Kuhl DE, Alavi A, Hoffman EJ, Phelps ME, Zimmerman RA, Obrist WD, Bruce DA, Greenberg JH, Uzzell B. Local cerebral blood volume in head-injured patients. Determination by emission computed tomography of 99mTc-labeled red cells. J Neurosurg. 1980; 52(3):309–320. [PubMed: 7359185]

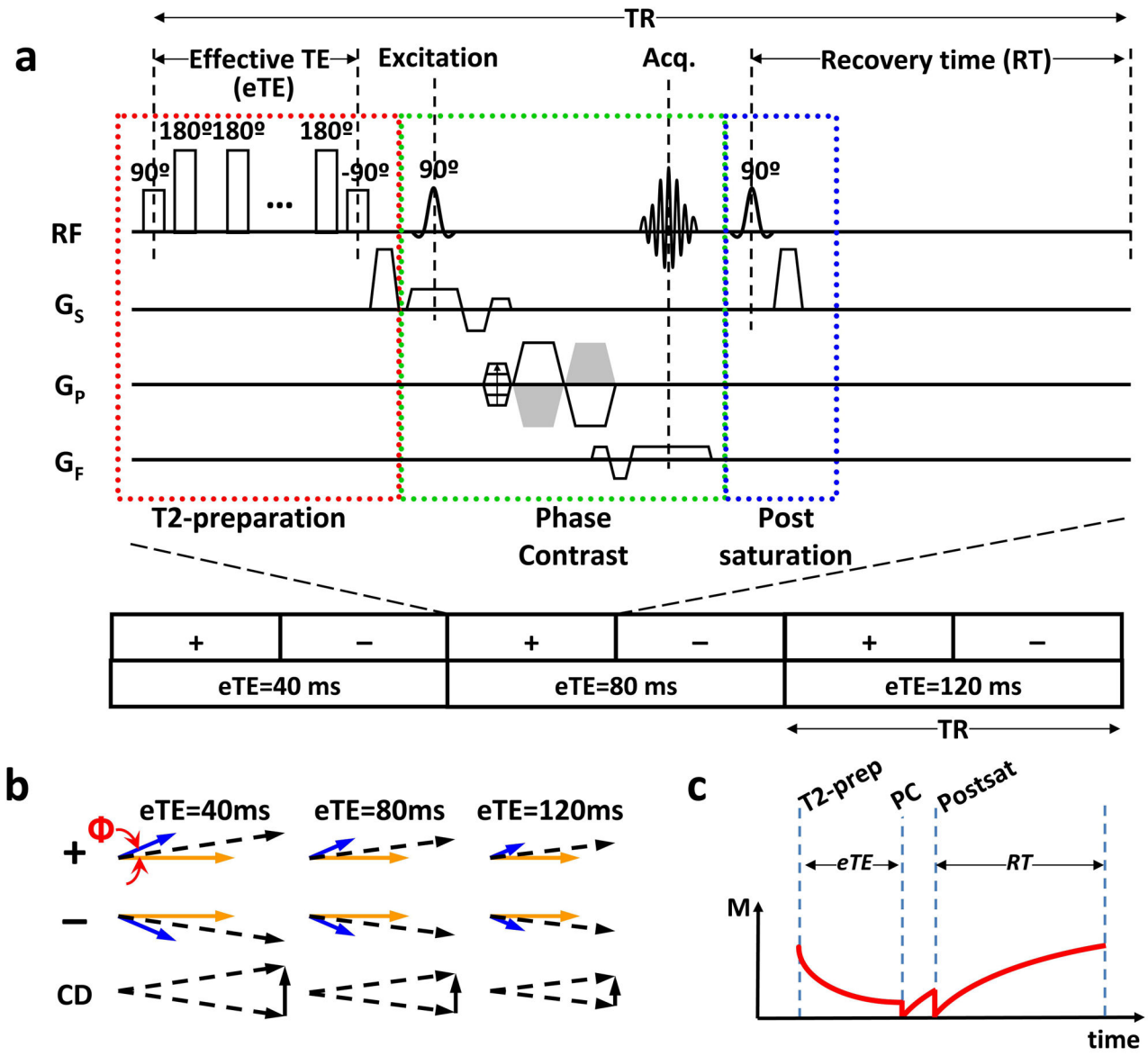

Figure 1.

Pulse sequence of TRU-PC MRI. (a) The pulse sequence of TRU-PC, made up of a combination of three components: a T2-preperation module (red box), a Phase-Contrast module (green box), and a Post-saturation module (blue box). The phase-contrast module allows for the separation of blood and tissue via the bipolar gradient applied in '+' or '−' orders. Here, '+' means positive lobe first. '−' means negative lobe first (see green box). The T2-preperation with length eTE provides the T2 weighting. Three different T2-prep schemes (40, 80, and 120 ms) are played out. The post-saturation pulse resets the magnetization. (b) Magnetization vectors for blood (blue) and tissue (yellow) compartments, and their summation (black dashed arrows). Φ is the phase shift of the flowing spins. The complex difference (CD) between '+' and '−' schemes is represented by the solid black arrow, and decreases in magnitude with each eTE. (c) Evolution of magnetization during one TR period. Only the magnetization component relevant for TRU-PC signal is plotted.

This corresponds to transverse magnetization during the T2-preparation period and longitudinal magnetization during the phase-contrast and post-saturation periods. PC = phase-contrast.

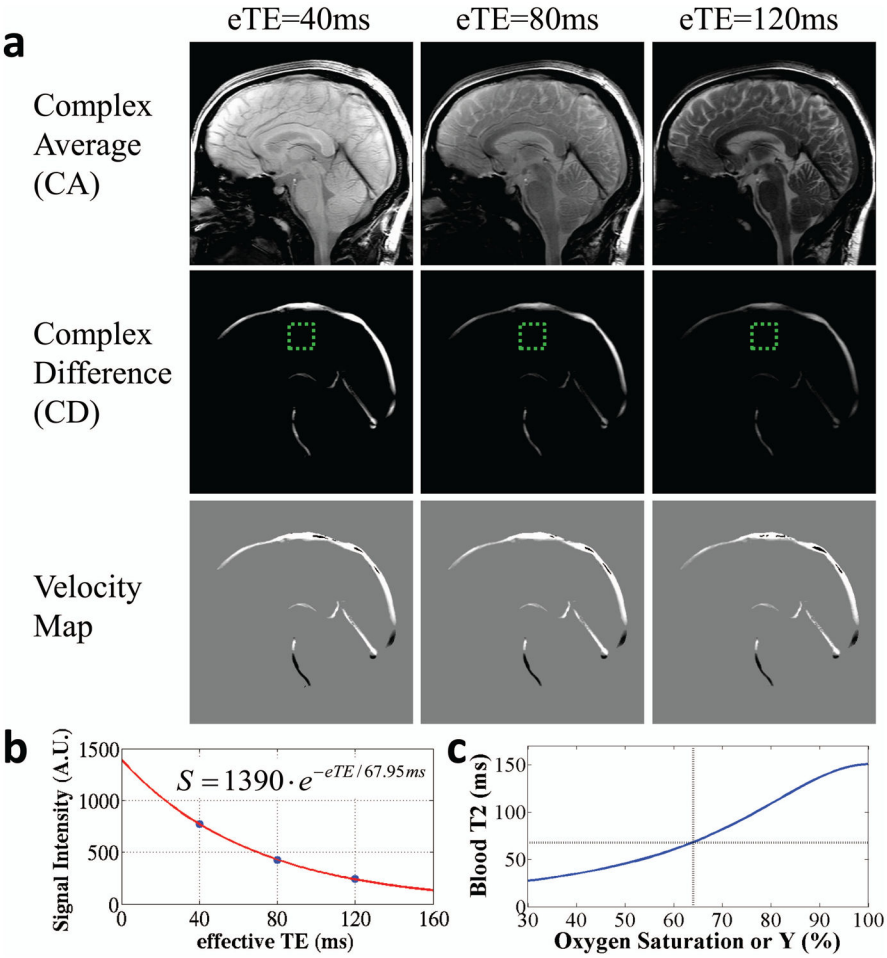

Figure 2.

Representative results of TRU-PC MRI. (a) TRU-PC images acquired with eTE=40, 80, and 120 ms. The complex average (CA) image contains both blood and tissue signal and decays appreciably with eTE. The complex difference (CD) is weighted by the amount of blood in the voxel as well as the velocity component along the encoding direction (anterior-posterior in this study). For voxels with flow velocity perpendicular to the encoding direction, the CD signal is relatively low even with high blood volume. The velocity map is obtained from the phase difference between '+' or '−' gradient-encoding schemes and does not vary with eTE. Vessels flowing from anterior to posterior show a positive (bright) velocity; those flowing from posterior to anterior show a negative (dark) velocity. Vessels whose flow is perpendicular to anterior-to-posterior direction will have 0 (gray) velocity in this image. The green dashed box indicates a region where the noise level is typically assessed from. (b) A representative plot of CD signal as a function of eTE. Blue symbols indicate experimental data. Red curve indicates the fitting curve. The fitted equation is shown in the inset. (c) The extracted blood T_2 is converted to blood oxygen saturation using a calibration plot, shown here for Hct=41%.

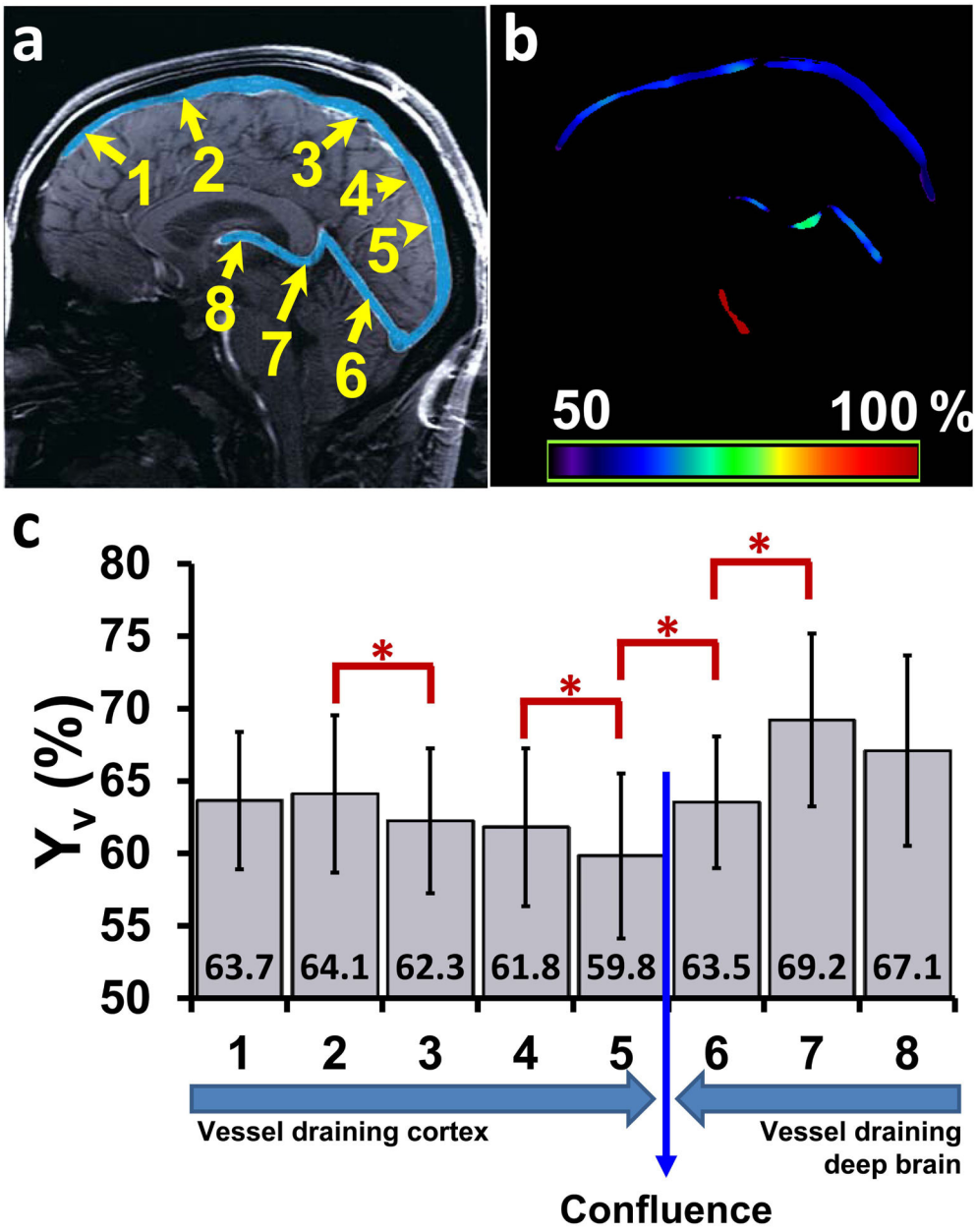

Figure 3.

Summary of TRU-PC results. (a) Illustration of eight ROIs on a mid-sagittal anatomic image. The major venous vessels are pseudo-colored in blue. The Superior Sagittal Sinus (SSS) is partitioned into 5 areas, where the direction of flow is from 1 to 5. ROI 6 represents the Straight Sinus (SS), ROI 7 covers the Great Vein (GV), and ROI 8 describes the Internal Cerebral Vein (ICV). The direction of flow through the deep veins is from ROI 8 to ROI 6, and takes a parallel trajectory to the SSS. (b) An oxygen saturation map acquired with TRU-PC MRI. The color bar describes the oxygen saturation from 50 to 100%. (c) Average Y_v in ROI 1–8 (N=22). Error bar = standard deviation. Red asterisks indicate significant (P<0.05)

differences between adjacent ROIs. The mean Y_v values are also listed at the bottom. The long arrows indicate flow directions.

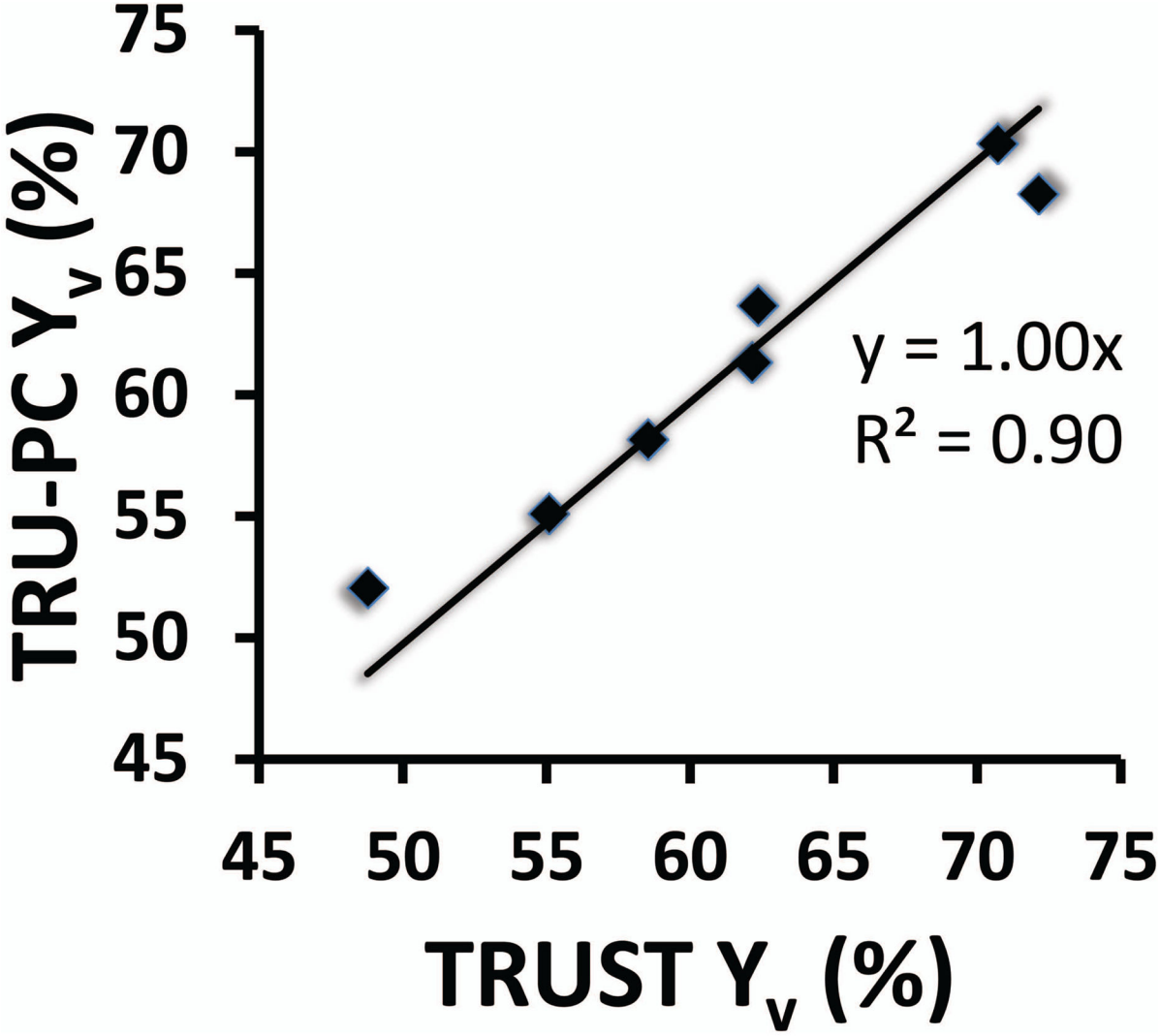

Figure 4.
Scatter plot between TRU-PC and TRUST Y_v values. Each symbol represents data from one subject. The linear fitting curve and the R^2 of the fitting are also shown.

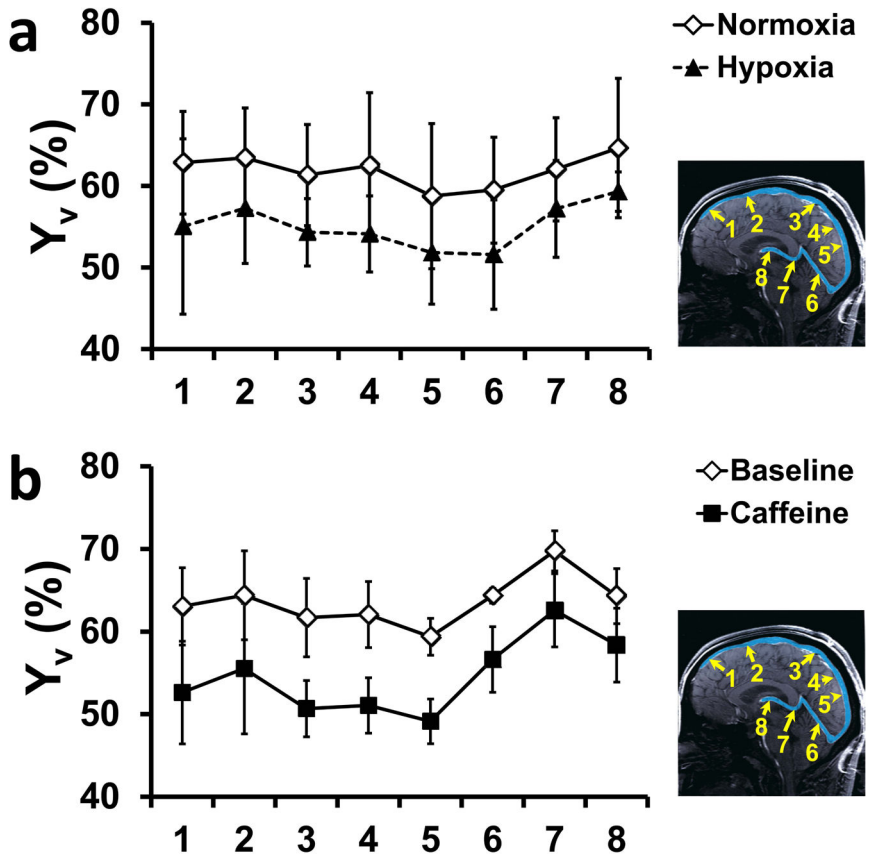

Figure 5.

Results of TRU-PC during physiologic challenges. (a) Y_v during normoxia and hypoxia in the 8 ROIs (see inset). N=5. (b) Y_v before and after caffeine ingestion in the 8 ROIs. N=5.

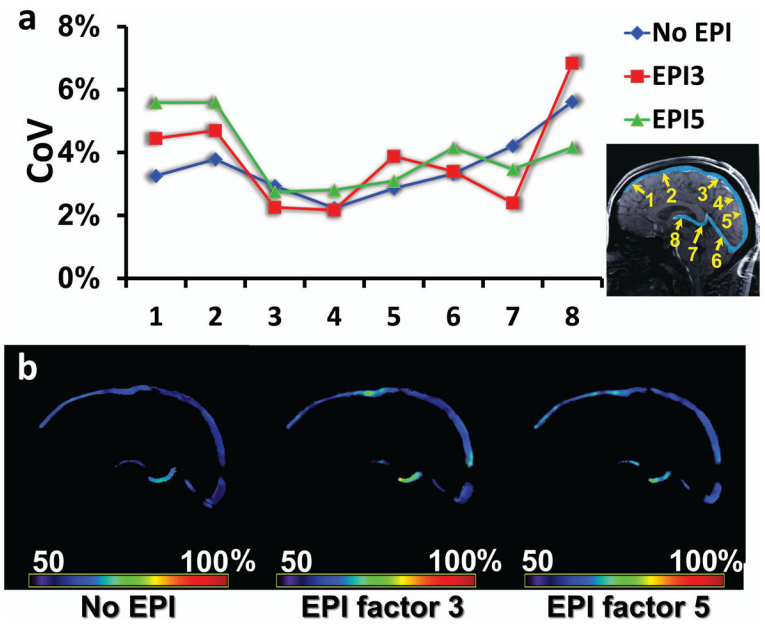

Figure 6.

Reproducibility of TRU-PC MRI. (a) Coefficient of Variation (CoV) for 8 regions (see inset). Data using different acquisition schemes are shown. The blue curve represents the standard (no EPI, or EPI factor 1) TRU-PC, the red curve represents the EPI-factor 3 TRU-PC, and the green curve represents the EPI-factor 5 TRU-PC. There is no significant difference between the CoV values for different acquisition schemes. (b) Representative TRU-PC Y_v maps obtained using different acquisition scheme. From Left to Right: standard (no EPI) TRU-PC, EPI-factor 3 TRU-PC, and EPI-factor 5 TRU-PC. The color bar describes the oxygen saturation from 50 to 100%.

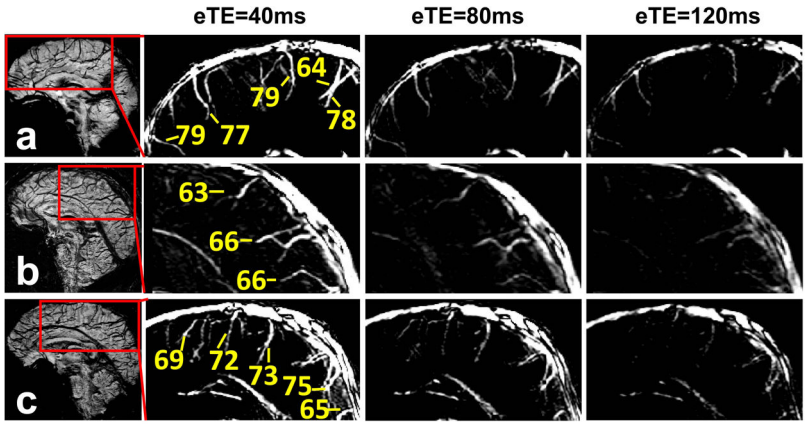

Figure 7.

TRU-PC applied to pial veins. Three healthy subjects were studied and the data are individually shown in Panels a through c. Left-hand image in each panel: A sagittal SWI image showing dark veins in contrast to bright tissue signal. The SWI image was used for localization of veins in the TRU-PC image. The red box indicates the region chosen for the subsequent TRU-PC analysis. The zoomed TRU-PC images for eTE 40, 80, and 120 ms show appreciable decay in the pial veins draining into the SSS. Estimated Y_v of discernible pial veins are listed in the image.

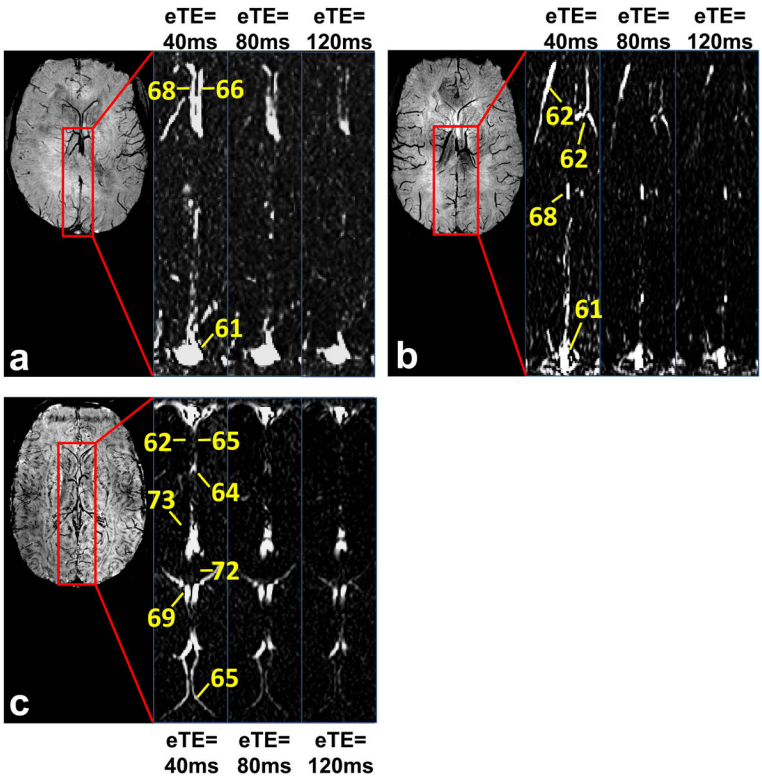

Figure 8.

TRU-PC applied to deep veins. Three healthy subjects were studied and the data are individually shown in Panels a through c. Left-hand image in each panel: An axial SWI image showing the deep veins of the brain. The red box indicates the region chosen for the subsequent TRU-PC analysis. The zoomed TRU-PC images for eTE 40, 80, and 120 ms show appreciable decay in all vessels specified. Estimated Y_v of discernible veins are listed in the image.

Table 1

Physiologic responses to hypoxia challenge (Mean ± SD).

FiO_2	EtO_2 (mmHg)	Y_a (%)	Y_v (%)
21%	138 ± 3	99 ± 1	61.7 ± 5.9
13%	81 ± 3	90 ± 4	55.1 ± 5.0
Difference	56 ± 4	7.8 ± 3.8	6.6 ± 3.8

FiO_2 – Fraction of O_2 in inhaled air. EtO_2 – end-tidal O_2. Y_a – arterial oxygenation. Y_v – venous oxygenation.